Paper AAS 03-596

FORMATION FLIGHT NEAR L1 AND L2 IN THE SUN-EARTH/MOON EPHEMERIS SYSTEM INCLUDING SOLAR RADIATION PRESSURE

B.G. Marchand and K.C. Howell
School of Aeronautics and Astronautics
Purdue University
West Lafayette, IN 47907-1282

AAS/AIAA Astrodynamics Specialists Conference

Big Sky Resort, Big Sky, Montana, August 3-7, 2003

AAS Publications Office, P.O. Box 28130, San Diego, CA 92198

AAS 03-596

FORMATION FLIGHT NEAR L_1 AND L_2 IN THE SUN-EARTH/MOON EPHEMERIS SYSTEM INCLUDING SOLAR RADIATION PRESSURE

B.G. Marchand[†] and K.C. Howell[‡]

The concept of formation flight of multiple spacecraft, near the libration points of the Sun-Earth/Moon (SEM) system, offers as many possibilities for space exploration as technical challenges. The initial phase of this research effort focused on the dynamics and control of formation flight in the circular restricted three-body problem (CR3BP). In the present phase, these results are transitioned into the more complete *n*-body ephemeris model to incorporate other gravitational perturbations as well as solar radiation pressure (SRP). The continuous control techniques previously applied in the CR3BP are successfully implemented in the SRP perturbed *n*-body ephemeris model. In addition, closer inspection of the flow corresponding to the stable and center manifolds near the reference halo orbit, reveals some potentially interesting nominal motions as well as some discrete control strategies for deployment. Furthermore, some of the control implementation issues associated with formation keeping of natural vs. non-natural configurations are addressed.

INTRODUCTION

Much of the available research on formation flight focuses on Earth orbiting configurations [1-17], where the influence of other gravitational perturbations can be safely ignored. However, renewed interest in formations that evolve near the vicinity of the Sun-Earth libration points has inspired new studies regarding formation keeping in the three-body problem [18-31]. Some of these investigations focus on the simplified circular restricted three-body problem (CR3BP) [18-22]. Howell and Marchand [18] consider linear optimal control, as applied to nonlinear time varying systems, as well as nonlinear control techniques,

[†] Ph.D. Student, School of Aeronautics and Astronautics, Purdue University, West Lafayette, IN 47907.
[‡] Professor, School of Aeronautics and Astronautics, Purdue University, West Lafayette, IN 47907.

including input and output feedback linearization. These control strategies are applied to a two spacecraft formation where the chief spacecraft evolves along a three-dimensional periodic halo orbit near the L_2 libration point. A detailed study of the nominal formation keeping costs over a 6-month period is presented for two types of configurations; for a constant relative separation distance, the chief-deputy line is assumed to remain (a) fixed relative to the rotating frame, or (b) fixed relative to the inertial frame. This particular effort does not constitute the only application of continuous control techniques in the CR3BP. Scheeres and Vinh [19] develop a non-traditional yet innovative continuous controller, based on the local eigenstructure of the linear system, to achieve bounded motion near the vicinity of a halo orbit. Although the latter approach is not suitable for precise formation keeping, nor is it necessarily the optimal way of achieving boundedness, it does achieve other goals that may be more important for other types of missions. In particular, the natural winding frequency of the spacecraft around the reference halo orbit is significantly increased. This is consistent with one of the stated requirements for TPF, where the formation is required to achieve a particular rotation rate that is not consistent with the natural dynamics near this region of space.

Other research efforts have also focused on the effectiveness of continuous control techniques in the general CR3BP, though not in the vicinity of the libration points. Gurfil and Kasdin consider both LQR techniques [20] and adaptive neural control [21] for formation keeping in the CR3BP. The second approach, described in [21], incorporates uncertainties introduced by modeling errors, inaccurate measurements, and external disturbances. Luquette and Sanner [22] apply adaptive nonlinear control to address the same sources of uncertainties in the nonlinear CR3BP.

Formations modeled in the CR3BP do represent a good starting point. However, ultimately, any definitive formation keeping studies must be performed in the *n*-body ephemeris model, where the time invariance properties of the CR3BP are lost and, consequently, precisely periodic orbits do not exist near the libration points. Hamilton [23] and Folta et al. [24] consider linear optimal control for formation flight relative to Lissajous trajectories, as determined in the ephemeris model. However, the evolution of the controlled formation is approximated from a linear dynamical model relative to the integrated reference orbit. Finally, Howell and Barden [25-28] also investigate formation flying near the vicinity of the libration points in the perturbed Sun-Earth/Moon system but their results are determined in the full nonlinear ephemeris model. Initially, their focus is the determination of the natural behavior on the center manifold near the libration points and the first step of their study captures a naturally occurring six-satellite formation near L_1 or L_2 [25]. Further analysis considers strategies to maintain a planar formation of the six vehicles in an orbit about the Sun-Earth L_1 point [26-28], that is, controlling the deviations of each spacecraft relative to the initial formation plane. A discrete station keeping/control approach is devised to force the orientation of the formation plane to remain fixed inertially. An alternate approach is also implemented by Gómez et al. [29]

in a study of the deployment and station keeping requirements for the TPF nominal configuration. Their analysis is initially performed in a simpler model but the simulation results are transitioned into the ephemeris model.

In the present investigation, the effectiveness of the continuous control techniques developed in [18] is successfully transitioned into the perturbed *n*-body ephemeris model. Mathematically, this is a sound approach to enforce non-natural formations. However, an actual formation flight mission may be required to rely on discrete control. Hence, the present study also considers two types of impulsive control. The first is a basic targeter approach that is, in concept, similar to that implemented by Howell and Barden [26-28] in the ephemeris model. This particular controller is applied here to an inertially fixed non-natural formation. Also, the station keeping techniques previously implemented by Howell and Keeter [30] and Gómez et al. [31], based on a Floquet controller, are adapted here to the formation keeping problem. In particular, the Floquet controller is applied to study naturally existing formations near the libration points and the potential deployment into such configurations.

DYNAMICAL MODEL

Background

In this investigation, the standard form of the relative equations of motion for the *n*-body problem, as formulated in the inertial frame $\left(\hat{X}-\hat{Y}-\hat{Z}\right)$, is employed. Hence, the dynamical evolution of each vehicle in the formation is governed by

$$ {}^{I}\ddot{\overline{r}}^{P_2P_s} = -\frac{\mu_q}{\left(r^{P_2P_s}\right)^3} + \sum_{j=1,j\neq 2,s}^{N} \mu_j \left(\frac{\overline{r}^{P_sP_j}}{\left(r^{P_sP_j}\right)^3} - \frac{\overline{r}^{P_2P_j}}{\left(r^{P_2P_j}\right)^3} \right) = \overline{f}_{grav}^{(P_s)} . \tag{1.1} $$

For notational purposes, let P_2 denote the central body of integration, in this case the Earth. Then, P_s represents the spacecraft, and the sum over j symbolizes the presence of other gravitational perturbations. The effects of solar radiation pressure (SRP) are also incorporated. The SRP force vector, as discussed by McInnes [32], can be modeled as

$$ \overline{f}_{srp}^{(P_s)} = \frac{kS_0A}{m_sc}\left(\frac{{D_0}^2}{d^2}\right)\cos^2\beta\,\hat{n}\,, \tag{1.2} $$

where k denotes the absorptivity of the spacecraft surface ($k=2$ for a perfectly reflective surface), S_0 is the energy flux measured at the Earth's distance from the Sun [W/m^2], D_0 is the mean Sun-Earth distance

[km], A represents the constant spacecraft effective cross sectional area [km^2], c is the speed of light [km/sec], m_s is the spacecraft mass [kg], β is the angle of incidence of the incoming photons, $\hat{n}$ denotes the unit surface normal, and d [km] represents the Sun-spacecraft distance. The sample spacecraft implemented in this study is modeled after the TPF combiner spacecraft, assuming a 25-meter diameter and a spacecraft mass of 700 kg. The SRP force parameters are summarized in Table 1.

Table 1 – TPF Combiner S/C Parameters

k	1.4	c	299792.458 km/sec	A	4.9087×10^{-4} km^2
S_0	1.358×10^{3} W/m^2	D_0	1.49597870×10^{8} km	m_s	700 kg

Suppose that the spacecraft is modeled as a flat plate. It is immediately obvious, from Equation (1.2), that the highest impact due to SRP occurs when the plate is normal to the incident photons, $\beta = 0^\circ$ and $\hat{n} = \bar{d} / d$. In this study, it is assumed that the vehicle is always oriented such that $\beta = 0^\circ$. In general, the inclusion of solar radiation pressure into the model has the most noticeable effect when the spacecraft mass is small relative to the effective area, as deduced from Equation (1.2). For instance, suppose the chief spacecraft in a formation evolves along a "halo" orbit near L_2, as determined in the Sun-Earth/Moon ephemeris model. If the mass of the spacecraft is 3500 kg, the impact of the SRP force on the path of the vehicle is barely noticeable, compared to the effect on a 700 kg spacecraft, as observed from Figure 1.

To further illustrate the effects of the addition of SRP on the dynamical model, consider the TPF combiner spacecraft described by the parameters in Table 1. Figure 2 illustrates the impact of the choice of dynamical model on a "halo" orbit near the instantaneous L_2 point of the Sun-Earth system, as observed in the rotating libration point (RLP) frame. The top left trajectory represents a halo orbit, with $A_z = 200,000$ km, as determined in the CR3BP. The top right figure depicts the same trajectory but transitioned into the ephemeris model (no periodicity). The orbit in the bottom left figure is also associated with the Sun-Earth ephemeris model but as perturbed by the Moon. Finally, the bottom right represents the same trajectory in the Sun-Earth/Moon system but includes SRP effects. Clearly, the dynamical model has a visible impact on the orbit. However, if the trajectory illustrated in the bottom right of Figure 2 represents the path of the chief spacecraft in a formation, the actual impact on the formation keeping cost is miniscule. For example, a 100-km formation of two spacecraft constrained to be aligned with the inertial y-axis $\left(\hat{Y}\right)$, over a period of 180 days, requires a nominal cost of 0.3272 m/sec in the absence of SRP in the ephemeris system. Including SRP in the dynamical model, as described in the following discussion, increases the cost to 0.3348 m/sec.

Control of Relative Motion in the Presence of SRP

The equations of motion for both the chief and deputy spacecraft may be expressed in the following form,

$$ {}^{I}\ddot{\bar{r}}_{I}^{P_2 C} = \bar{f}_{grav}^{(C)} + \bar{f}_{srp}^{(C)} + \bar{u}_C(t) = \bar{f}^{(C)} + \bar{u}_C(t), \tag{1.3} $$

$$ {}^{I}\ddot{\bar{r}}_{I}^{P_2 D_i} = \bar{f}_{grav}^{(D_i)} + \bar{f}_{srp}^{(D_i)} + \bar{u}_{D_i}(t) = \bar{f}^{(D_i)} + \bar{u}_{D_i}(t), \tag{1.4} $$

where $\bar{u}_C(t)$ and $\bar{u}_{D_i}(t)$ denote the control accelerations required to maintain the desired nominal configuration, and $\bar{f}^{(C)}$ and $\bar{f}^{(D_i)}$ represent the net force acting on the chief spacecraft and the i^{th} deputy vehicle, respectively. The numerical integration for all vehicles in the formation is performed in terms of inertial coordinates such that, for instance, $\bar{r}^{P_2 D_i} = x_i \hat{X} + y_i \hat{Y} + z_i \hat{Z}$. Thus, the vehicle velocities and accelerations are associated with the inertial frame (*I*).

The chief spacecraft, or center of the formation, is assumed to evolve along a quasi-periodic Lissajous trajectory. Since this is a naturally existing solution in this regime, the baseline control acceleration $\bar{u}_C(t)$ is zero. The relative equations of motion for the i^{th} deputy, then, are easily determined by subtracting Equation (1.3) from (1.4),

$$ {}^{I}\ddot{\bar{r}}_{I}^{CD_i} = \left(\bar{f}_{grav}^{(D_i)} - \bar{f}_{grav}^{(C)}\right) + \left(\bar{f}_{srp}^{(D_i)} - \bar{f}_{srp}^{(C)}\right) + \bar{u}_{D_i}(t) = \Delta\bar{f}^{(D_i)} + \bar{u}_{D_i}(t). \tag{1.5} $$

The vector $\bar{r}^{CD_i}$ denotes the position of the i^{th} deputy relative to the chief spacecraft while $\Delta\bar{f}^{(D_i)}$ represents the relative net force vector. Let $\bar{\rho}$ represent the desired nominal path of the deputy spacecraft, then, $\dot{\bar{\rho}}$ designates the nominal velocity vector, and $\bar{u}_{D_i}^{\circ}(t)$ denotes the associated nominal control effort such that,

$$ \ddot{\bar{\rho}} = \Delta\bar{f}^{D_i^{\circ}} + \bar{u}_{D_i}^{\circ}(t). \tag{1.6} $$

The superscript "∘" denotes evaluation on the nominal solution $\left(\bar{\rho}, \dot{\bar{\rho}}\right)$. Then, the error dynamics are easily determined by subtracting the nominal motion in Equation (1.6) from (1.5),

$$ {}^{I}\ddot{\bar{e}} = {}^{I}\ddot{\bar{r}}_{I}^{CD_i} - \ddot{\bar{\rho}} = \left\{\Delta\bar{f}^{D_i} - \Delta\bar{f}^{D_i^{\circ}}\right\} + \left\{\bar{u}_{D_i} - \bar{u}_{D_i}^{\circ}\right\} = \delta\Delta\bar{f}^{D_i} + \delta\bar{u}_{D_i}(t). \tag{1.7} $$

In the above equation, the nominal solution corresponds to the zero vector, i.e., $\bar{e}(t) = \bar{0}$. Howell and Marchand [18] establish the effectiveness of an input feedback linearization (IFL) control approach in the CR3BP. This continuous control technique is applied here to the ephemeris model formulation. Consistent

with the previous definition of the IFL controller [18], suppose that a critically damped error response, characterized by a natural frequency ω_n, is desired. Then, the differential control input, $\delta\bar{u}_{D_i}(t)$, measured relative to the nominal control acceleration $\bar{u}_{D_i}^{\circ}(t)$, is determined as

$$\delta\bar{u}_{D_i}(t) = -\delta\Delta\bar{f} - 2\omega_n {}^{I}\dot{\delta}\bar{e} - \omega_n^2\delta\bar{e} \ . \tag{1.8}$$

The total control effort is then the sum of the nominal control input, $\bar{u}_{D_i}^{\circ}(t)$, and the differential control acceleration, $\delta\bar{u}_{D_i}(t)$.

As an example, define a two spacecraft 100-km formation that is constrained to remain aligned with the inertial *y*-axis ($\hat{Y}$) at all times. That is, while the chief spacecraft evolves along the reference "halo" orbit represented by the bottom right trajectory in Figure 2, the deputy is always located 100 km away from the chief spacecraft along the inertial *y*-direction. For an arbitrary injection error, relative to $\bar{\rho}$ and $\dot{\bar{\rho}}$, of the form $\delta\bar{r} = \left(7\hat{X} - 5\hat{Y} + 3.5\hat{Z}\right)$ km in position and $\delta^{I}\dot{\bar{r}} = \left(\hat{X} - \hat{Y} + \hat{Z}\right)$ m/sec in velocity, it is clear, as observed from Figure 3, that the error response, based on the IFL controller, is not noticeably affected by the choice of model. The formation keeping cost, over 180 days, changes only slightly between models. Transitioning the orbit into the ephemeris model, with or without the Moon, decreased the cost from 4.00 m/sec in the CR3BP to 3.86 m/sec. However, adding solar radiation pressure increased the net formation keeping cost slightly to 3.88 m/sec.

CONTINUOUS VERSUS DISCRETE CONTROL

Background

Based on results from previous investigations, [18, 20-22] it appears that it is possible, at least computationally, to achieve precise formations in the CR3BP <u>if</u> continuous control is both available and feasible. Howell and Marchand [18] demonstrate that, to maintain two spacecraft separated by 5000 km, a 2000 kg vehicle would nominally require thrust levels ranging between 0.86 and 2.10 mN, as determined in the CR3BP for a 200,000 km reference halo orbit. If the separation distance is reduced to 100 meters, that thrust level is reduced to 1.7×10^{-5} to 4×10^{-5} mN. The low continuous thrust levels that are required, near the libration points, to maintain a small formation like TPF presently represent a technical challenge. Furthermore, although continuous control approaches are mathematically sound, the science goals of deep space missions may impose a series of constraints that eliminate continuous control as a feasible option. Some also suggest that maintaining a precise formation is, perhaps, ultimately not as critical as generating precise knowledge of the relative position of each spacecraft in the formation. In these cases, a discrete formation keeping strategy may represent an important capability.

Investigation of Various Control Strategies

In this study, three different discrete control strategies are considered for formation keeping. All of these rely on knowledge of the linearized dynamics associated with the reference orbit, but incorporate the nonlinear response of the vehicle. In this case, the reference orbit is the path of the chief spacecraft, assumed to evolve along a 200,000 km halo orbit. The deputy dynamics, then, are modeled as a perturbation relative to the reference orbit. The success of a particular control strategy depends, in part, on the nominal motion that is required of the deputy.

In the first method, the nominal path of the deputy spacecraft is characterized as an inertially fixed distance and orientation, relative to the chief spacecraft. Since this type of motion does not exist naturally near the libration points, continuous control is necessary to precisely enforce the formation for the duration of the mission. Here, instead of applying continuous control, the path of the deputy is divided into segments. At the beginning of each segment, an impulsive maneuver is implemented that targets the nominal state at the end of the segment. If the nominal separation between the chief and deputy spacecraft is small, this approach proves to be effective. That is, the maximum error, as measured relative to the nominal state, incurred between maneuvers is only within a few centimeters.

The remaining two controllers are derived from Floquet analysis, based on the reference orbit, and are designed to remove the unstable component of the relative state, as well as two of the four center subspace modes that are associated with the reference orbit. The path of the deputy, then, is representative of a synthesis between the stable and center flows. In contrast with the first method, these two controllers do not target a non-natural reference motion. Instead, these control schemes nominally place the deputy spacecraft on a naturally existing path that exhibits nearly periodic behavior, bounded motion, or quasi-periodic motion relative to the chief spacecraft. The control essentially seeks to return the deputy to this natural path.

Continuous control is also a topic of interest in this investigation – as a step toward the ultimate goal, that is, the development of an effective optimal discrete controller. For instance, one aspect of the present study is nonlinear optimal control. The focus is not actually the controller itself, but rather the identification of simple and yet efficient numerical methods to solve the associated two-point boundary value problem. The highly nonlinear nature of the equations makes this a very difficult task and, as such, this particular phase of the study represents an ongoing effort. Ultimately, this undertaking is only a building block towards identifying an optimal nonlinear discrete controller and the numerical methods required to solve this problem.

DISCRETE CONTROL IN THE EPHEMERIS MODEL

Driven by control and/or implementation requirements, some new consideration is warranted concerning the degree of accuracy to which the formation can be maintained via discrete impulses. An LQR controller, based on a discrete time system, yields the optimal magnitude of each differential control impulse at specified time intervals. However, the value of the nominal control input that must be added is still assumed to be continuously available. So, in a truly discrete control strategy, how often must an impulsive maneuver be incorporated to maintain the desired configuration to some acceptable degree of accuracy, even in the presence of external perturbations?

Targeting a Nominal Relative State

Consider the case of a formation of two spacecraft separated by 100 km, constrained to remain aligned with the inertial *y*-axis ($\hat{Y}$) at all times. In the absence of any external perturbations, a continuous control approach via IFL, as discussed by Howell and Marchand [18], requires 0.3348 m/sec of total ΔV over a period of 180 days. How much will the formation diverge if the control input is discretized over a period of hours, or even days? Consider the general form of the solution to the linear system,

$$\begin{bmatrix} \delta\overline{r}_{k+1} \\ \delta\overline{v}_{k+1} \end{bmatrix} = \Phi\left(t_{k+1}, t_k\right) \begin{bmatrix} \delta\overline{r}_k \\ \delta\overline{v}_k \end{bmatrix} = \begin{bmatrix} A_k & B_k \\ C_k & D_k \end{bmatrix} \begin{bmatrix} \delta\overline{r}_k \\ \delta\overline{v}_k + \Delta\overline{v}_k \end{bmatrix}, \tag{1.9}$$

where $\Phi\left(t_{k+1}, t_k\right)$ denotes the state transition matrix, from time t_k to time t_{k+1}, associated with the nominal Lissajous orbit along which the chief spacecraft is assumed to evolve. The symbol δ denotes a perturbation relative to the nominal Lissajous trajectory and $\Delta\overline{v}_k$ represents an impulsive maneuver applied at the beginning of the k^{th} segment, marked by t_k. Controlling the position of the deputy spacecraft relative to the chief to a constant vector, as observed in the inertial frame, is equivalent to targeting a particular constant perturbation $\delta\overline{r}_{k+1}$ relative to the inertial frame. An impulsive maneuver of the form

$$\Delta v_k = B_k^{-1}\left(\delta\overline{r}_{k+1} - A_k\delta\overline{r}_k\right) - \delta\overline{v}_k, \tag{1.10}$$

will accomplish the goal in the linear system. A precise implementation of this scheme in the nonlinear system requires that the maneuvers be differentially corrected over each segment as discussed by Howell and Barden [26-28]. However, the simple expression in Equation (1.10) does accomplish the objective, provided the length of each segment, $\Delta t_k = t_{k+1} - t_k$, is sufficiently small. This observation is deduced from Figure 4. The maneuver strategies associated with each curve in Figure 4 are illustrated in Figure 5. Not surprisingly, the total Δv computed via the discrete control approach converges on the cost determined from the IFL continuous controller ($\Delta v = 0.3348$ m/sec) as the interval between maneuvers decreases.

Note, from Figure 4, that during the wait period between maneuvers the trajectory diverges quickly from the pre-specified nominal path. Naturally, the maximum error incurred during each segment decreases as the scheduled time between maneuvers decreases. In spite of this trend, these results indicate that, if the nominal radial separation is large, continuous control is still required if a good level of accuracy is desired. Smaller formations, on the other hand, can benefit from a discrete approach. For instance, consider a formation characterized by a 10-meter separation between the chief and deputy spacecraft. In particular, let the nominal formation be defined by $\bar{\rho} = (10 \text{ m})\hat{Y}$ and $\dot{\bar{\rho}} = \bar{0}$. As depicted in Figure 6, the maximum deviation achieved between maneuvers is significantly smaller, dropping below one centimeter for maneuvers scheduled at least every 2 days. The maneuver history for each of the examples in Figure 6 is illustrated in Figure 7. Note that the magnitude of the individual maneuvers is still extremely small, which is consistent with the natural sensitivity to small changes in this region of space. Hence, the error introduced in any attempt to physically implement such a small maneuver may offset the benefits. The results in Figure 6 also raise another issue. In particular, for a given maneuver interval, how large can the nominal relative separation be such that the desired configuration is maintained within some acceptable tolerance (e.g., one centimeter)? As observed from Figure 8, formation separations of up to 50 meters can be achieved to within a centimeter at all times, if a maneuver is performed once a day. If that interval is doubled to once every two days, then the maximum relative separation recommended drops to 15 meters.

Clearly, achieving the desired nominal configuration to extreme accuracy requires maneuvers that are fairly close to each other. However, this fact introduces yet another difficulty. As the maneuvers become more closely spaced they also decrease in size. The magnitude of the maneuvers illustrated in Figure 7 is already extremely small (10^{-6} m/sec). So, regardless of whether continuous or discrete control is available, accurately maintaining a non-natural nominal configuration, with small relative separations, is apparently not achievable with the technology presently available. Since the natural flow in this region of space is constantly acting against these non-natural configurations, the relative error increases rapidly if these small maneuvers are not accurately implemented. Conversely, formations that take advantage of the natural flow near the reference orbit require minimal station keeping beyond the initial injection maneuver.

Formations that Exploit the Center + Stable Manifolds

The center manifold that exists in the immediate vicinity of the reference halo orbit allows for a variety of natural motions that could prove beneficial for formation flight missions. To numerically identify these regions, it is necessary to understand the eigenstructure associated with the reference orbit. To that end, the analysis of the center manifold as presented here employs the CR3BP, where the reference orbit is defined as a three-dimensional, periodic halo orbit. The natural formation dynamics in the vicinity of the reference

orbit are studied in detail. Once a suitable set of nominal configurations is identified, the results are easily transitioned into the ephemeris model previously described via a differential corrections process.

Floquet Analysis

Let $\bar{x}^*(t)$ denote the state vector, at time *t*, along a reference halo orbit near L_1 or L_2 in the CR3BP and let $\delta\bar{x}(t)$ denote a perturbation relative to $\bar{x}^*(t)$. Since the following analysis is performed in the CR3BP, these vectors are both expressed in terms of rotating coordinates consistent with the standard definition of the synodic rotating frame. In this frame, $\hat{x}$ is directed from the Sun to the Earth/Moon barycenter, $\hat{z}$ is normal to the plane of motion of the primaries, and $\hat{y}$ completes the right handed triad. The velocity elements of the vectors $\bar{x}^*(t)$ and $\delta\bar{x}(t)$ are both associated with an observer fixed in the rotating frame.

In terms of the linearized dynamics, the evolution of the perturbation vector $\delta\bar{x}(t)$ is governed by the state transition matrix, $\Phi(t,0)$, such that

$$\delta\bar{x}(t) = \Phi(t,0)\delta\bar{x}(0). \tag{1.11}$$

Since the reference orbit is *T*-periodic, the state transition matrix admits a Floquet decomposition [30-31] of the form

$$\Phi(t,0) = P(t)e^{Bt}P(0)^{-1}, \tag{1.12}$$

where $P(t) = P(t+T)$ is a periodic matrix, $P(0)$ is the identity matrix, and B is a constant matrix. The matrix B is easily evaluated from the monodromy matrix, $\Phi(T,0)$, as

$$B = \frac{1}{T}\log\left|\Phi(T,0)\right|. \tag{1.13}$$

To develop a better understanding of the dynamics near the reference orbit, it is useful to express B in terms of its real Jordan form such that

$$B = SJS^{-1}, \tag{1.14}$$

where J is a block diagonal matrix formed by the real and imaginary parts of the eigenvalues of B, and the columns of S represent the real and imaginary parts of the associated eigenvectors. By substituting Equation (1.14) into (1.12), and properly rearranging the resulting terms, it is clear that

$$\Phi(t,0)\{P(0)S\} = \{P(t)S\}e^{Jt}. \tag{1.15}$$

This leads to the definition of the Floquet Modal matrix,

$$E(t) = P(t)S = \Phi(t,0)E(0)e^{-Jt}. \tag{1.16}$$

Note that, since $P(t)$ is periodic, and S is a constant matrix, the modal matrix is also periodic with $E(0) = S$.

The reference halo orbits of interest in this study are inherently unstable. The six-dimensional eigenstructure of the B matrix is thus characterized by one unstable eigenvalue (γ_1), one stable eigenvalue (γ_2), and four eigenvalues associated with the center subspace. Two of these neutrally stable eigenvalues are purely imaginary (γ_3 and γ_4) and the remaining two are exactly equal to zero (γ_5 and γ_6). The eigenvalues of the *B* matrix are commonly denoted the Floquet exponents. The eigenvectors, or modes, associated with these eigenvalues are here defined as $\bar{s}_j$. Once these eigenvalues and eigenvectors are identified, the Floquet modes at each point along the orbit can be computed from Equation (1.16).

Now, at a point in time, the perturbation $\delta\bar{x}(t)$ can be expressed in terms of any six-dimensional basis. The Floquet modes ($\bar{e}_j$), defined by the columns of $E(t)$, form a non-orthogonal six-dimensional basis. Hence, $\delta\bar{x}(t)$ can be expressed as

$$\delta\bar{x}(t) = \sum_{j=1}^{6} \delta\bar{x}_j(t) = \sum_{j=1}^{6} c_j(t)\bar{e}_j(t), \tag{1.17}$$

where $\delta\bar{x}_j(t)$ denotes the component of $\delta\bar{x}(t)$ along the j^{th} mode, $\bar{e}_j(t)$, and the coefficients $c_j(t)$ are easily determined as the elements of the vector $\bar{c}(t)$ defined by

$$\bar{c}(t) = E(t)^{-1}\,\delta\bar{x}(t). \tag{1.18}$$

The Floquet analysis presented above is implemented by Howell and Keeter [30] and Gómez et al. [31] as the basis of a station keeping strategy for a single spacecraft evolving along a halo orbit. In their study, Howell and Keeter (following Gómez et al.) determine the impulsive maneuver scheme that is required to periodically remove the unstable component, $\delta\bar{x}_1$, of the perturbation, $\delta\bar{x}(t)$. For instance, let

$$\delta\bar{x}_n(t) = \sum_{j=2}^{6} \left(1 + \alpha_j(t)\right)\delta\bar{x}_j\,, \tag{1.19}$$

denote the desired perturbation relative to the reference orbit, where the $\alpha_j(t)$'s denotes some, yet to be determined, coefficients. Note that the limits of the summation range from 2 through 6 which implies that the unstable mode, $\bar{e}_1$, has been removed. The control problem, then, reduces to finding the impulsive maneuver, $\Delta\bar{v}(t)$, such that

$$\sum_{j=2}^{6}\left(1+\alpha_j(t)\right)\delta\bar{x}_j(t)=\sum_{j=1}^{6}\delta\bar{x}_j+\begin{bmatrix}0_3\\ \Delta\bar{v}\end{bmatrix}. \tag{1.20}$$

After some reduction, Equation (1.20) can be rewritten in matrix form as

$$\begin{bmatrix}\delta\bar{x}_{2r} & \delta\bar{x}_{3r} & \delta\bar{x}_{4r} & \delta\bar{x}_{5r} & \delta\bar{x}_{6r} & 0_3\\ \delta\bar{x}_{2v} & \delta\bar{x}_{3v} & \delta\bar{x}_{4v} & \delta\bar{x}_{5v} & \delta\bar{x}_{6v} & -I_3\end{bmatrix}\begin{bmatrix}\bar{\alpha}\\ \Delta\bar{v}\end{bmatrix}=\tilde{E}^*\bar{\alpha}^*=\delta\bar{x}_1, \tag{1.21}$$

where $\delta\bar{x}_{jr}$ refers to the first three elements of the vector $\delta\bar{x}_j$, $\delta\bar{x}_{jv}$ denotes the last three elements of $\delta\bar{x}_j$, and $\bar{\alpha}$ represents a 5×1 vector formed by the α_j coefficients in Equation (1.20). Howell and Keeter [30] identify the required $\Delta\bar{v}$ via a minimum norm solution. An exact solution is also considered in both [30] and [31] by constraining the maneuver to be performed along the Sun-Earth line $(\hat{x})$. Although this approach was originally devised for station keeping of the reference orbit, in this study, a modified version of the methodology provides much insight for formation keeping in the three-body problem. In particular, a discrete three-axis control is implemented that removes the components of $\delta\bar{x}$ associated with the unstable mode ($\delta\bar{x}_1$) and two of the four center modes ($\delta\bar{x}_3$ and $\delta\bar{x}_4$ or $\delta\bar{x}_5$ and $\delta\bar{x}_6$). The particular set of two center modes that is removed depends on the kind of formation that is sought.

In general, the center modes point towards other bounded solutions that exist in the vicinity of the reference halo orbit. For instance, modes $\bar{e}_3(t)$ and $\bar{e}_4(t)$ point towards a torus that is known to envelop the halo orbit, as illustrated in Figure 9. This two-dimensional torus exists both in the CR3BP and in the ephemeris model and represents a natural (unforced) solution to the nonlinear equations of motion. In fact, the surface illustrated in Figure 9 is associated with the ephemeris model. Hence, if the initial perturbation, $\delta\bar{x}(0)$, is entirely contained within the subspace spanned by $\bar{e}_3$ and $\bar{e}_4$, then the perturbed path, relative to the halo orbit, is bounded and evolves along a torus such as that illustrated in Figure 9. Now, suppose that $\delta\bar{x}(t)$ represents the relative dynamics of a deputy spacecraft. This implies that the chief S/C is assumed to evolve along the halo orbit. The relative path that defines the motion of the deputy is best visualized from the Figures 10 and 11. Relative to the chief spacecraft, Figure 10 depicts the surface along which the deputy evolves, while Figure 11 details the exact manner in which the evolution proceeds. In these figures, the chief S/C is always located at the origin. Note that the surface in Figure 10 self-intersects several times, but that is merely a product of the projection of the six-dimensional states onto three-dimensional configuration space. Furthermore, although the surface illustrated in Figure 10 is generated in the linear system, it is known to represent a natural solution to the nonlinear equations both in the CR3BP and in the ephemeris model, as illustrated in Figure 9.

If, instead, the initial state is entirely contained within the subspace spanned by $\bar{e}_5$ and $\bar{e}_6$, then the perturbed path corresponds to a neighboring halo orbit. A blend of subspaces reveals some interesting possible motion, however. The controller developed by Howell and Keeter is modified such that, at periodic time intervals, the unstable component of $\delta\bar{x}(t)$ is removed, along with two of the center modes. For instance, the $\Delta\bar{v}$ required to remove modes $\bar{e}_1$, $\bar{e}_3$, and $\bar{e}_4$ can be determined exactly from

$$\begin{bmatrix} \bar{\alpha} \\ \Delta\bar{v} \end{bmatrix} = \begin{bmatrix} \delta\bar{x}_{2\bar{r}} & \delta\bar{x}_{5\bar{r}} & \delta\bar{x}_{6\bar{r}} & 0_3 \\ \delta\bar{x}_{2\bar{v}} & \delta\bar{x}_{5\bar{v}} & \delta\bar{x}_{6\bar{v}} & -I_3 \end{bmatrix}^{-1} \left(\delta\bar{x}_1 + \delta\bar{x}_3 + \delta\bar{x}_4 \right). \tag{1.22}$$

Similarly, the $\Delta\bar{v}$ required to remove modes $\bar{e}_1$, $\bar{e}_5$, and $\bar{e}_6$ is exactly determined from

$$\begin{bmatrix} \bar{\alpha} \\ \Delta\bar{v} \end{bmatrix} = \begin{bmatrix} \delta\bar{x}_{2\bar{r}} & \delta\bar{x}_{3\bar{r}} & \delta\bar{x}_{4\bar{r}} & 0_3 \\ \delta\bar{x}_{2\bar{v}} & \delta\bar{x}_{3\bar{v}} & \delta\bar{x}_{4\bar{v}} & -I_3 \end{bmatrix}^{-1} \left(\delta\bar{x}_1 + \delta\bar{x}_5 + \delta\bar{x}_6 \right). \tag{1.23}$$

Either one of these controllers leads to motion that exhibits not only the overall features of the associated center subspaces, but also of the stable manifold that converges onto that region of space. As a direct result, the controllers described by Equations (1.22) and (1.23) not only define other potential nominal configurations, but also deployment into these configurations, as is demonstrated below.

Application: Floquet Controller to Deploy Into Quasi-Periodic Torus Formation

Consider a two-spacecraft formation where the chief spacecraft is assumed to evolve along a 200,000 km halo orbit near the Sun-Earth/Moon L_1 point. Both spacecraft are deployed and arrive simultaneously at different points along the *xz*-plane. Let the "arrival" point for both spacecraft be defined as the point where they cross the *xz*-plane near the reference orbit. The position of the deputy spacecraft upon arrival is similar to the chief but 50 meters off along the $+\hat{x}$ direction. The relative velocity of the deputy is not important, only the relative orientation of the two spacecraft is relevant. Once at the arrival point, the deputy spacecraft performs its first formation keeping maneuver, as determined from Equation (1.23). This maneuver is the largest and is meant to place the spacecraft state into the desired subspaces. The magnitude of the maneuver is approximately equal to the magnitude of the relative velocity of the deputy with respect to the chief. For this particular example, the initial relative velocity of the deputy is selected as $\bar{v} = \left(\hat{x} - \hat{y} + \hat{z}\right)$ m/sec. Thus, the deputy's first maneuver is $\left|\Delta\bar{v}_1\right| = 1.73$ m/sec. Thereafter, the trajectory of both the chief and deputy spacecraft requires a small deterministic $\Delta\bar{v}$ every 180 days (1 orbital period along the halo orbit). For the chief spacecraft, these are necessary to enforce the periodicity condition over 100 orbital periods (and may simply be a numerical artifact). All of these corrections – both for the chief and deputy – are on the order of 10^{-8} m/sec.

The resulting path is illustrated in Figure 12. The first leg of the path is characteristic of motion along the stable manifold, associated with mode 2, while the converged path is consistent with the motion associated with modes 5 and 6, previously illustrated in Figure 10.

Application: Floquet Controller to Deploy Into Nearly Periodic Formations

For the same reference halo orbit employed in the previous example, consider three deputies deployed along with the chief spacecraft. Each deputy spacecraft arrives simultaneously at a different location relative to the chief. In particular, the relative position vectors are 50 meters, 100 meters, and 140 meters along the +*x*-direction. Application of the Floquet controller described by Equation (1.22) leads to a nearly periodic formation. Once again, the first leg along the path of each deputy resembles motion along the stable manifold associated with the reference halo orbit. However, the converged path is nearly periodic, as observed from Figure 13. The resulting path is propagated for 10 revolutions of the reference halo orbit (1800 days). Beyond the initial injection maneuver, numerical corrections are implemented once every 180 days, although the magnitude is small (10^{-8} m/sec).

The converged segment of the path in Figure 13 reveals a variety of very nearly periodic solutions in the vicinity of the chief spacecraft. Since the controller forces these solutions to remain within a subspace spanned by $\bar{e}_2$, $\bar{e}_5$, and $\bar{e}_6$, the resulting path is not evolving solely along the halo family but rather along another type of nearly periodic motion in the vicinity of the reference halo orbit. To better visualize the potential configurations, Figure 14 illustrates eight deputies evolving along nearly periodic orbits. The actual path of each is expanding, but it does so very slowly. So, the individual orbits can be propagated for 100 revolutions of the reference halo and will still appear periodic. Let $\bar{r}(t)$ denote the vector formed by the position elements of $\delta\bar{x}(t)$. The orbits depicted in Figure 14 are obtained by applying the controller to a relative position vector of the form $\bar{r} = r_0\hat{y}$, where r_0 denotes some initial separation between the chief and deputy spacecraft. The rate of expansion of these orbits is more noticeable if the initial position vector originates anywhere else in the *yz*-plane. In fact, the rate of expansion reaches a maximum if the initial relative position vector is of the form $\bar{r} = r_0\hat{z}$. In this case, the resulting orbits appear nearly vertical and are illustrated in Figure 15 using a four spacecraft formation as an example. In the *yz*-projection, it is apparent that the expansion proceeds clockwise since, in this case, the reference orbit is a northern L_1 halo orbit. This is consistent with the direction of motion both along the halo family and the stable manifold in this region of space. Figure 16 further illustrates how the rate of expansion changes as the initial state is shifted throughout the *yz*-plane. The sphere at the origin (the location of the chief) is included only to aid in visualizing the path of the deputy. Note that with no initial *z*-component, the orbit of the vehicle appears periodic.

As an out-of-plane component is introduced into the initial state, the resulting trajectory blends the characteristics of the orbits in both Figures 14 and 15. Further propagating a nearly vertical orbit, characterized by $\bar{r}(0) = r_0\hat{z}$, over a period of 100 revolutions (49.2 years) yields the surface illustrated in Figure 17.

Natural String of Pearls Formation

Another natural formation that exists in the three-body problem (CR3BP or ephemeris model) is analogous to the "string of pearls" formation and is illustrated in Figure 18. The surface illustrated in Figure 18 is traced by a quasi-periodic Lissajous trajectory near the Sun-Earth/Moon L_2 point, as determined in the SRP perturbed *n*-body ephemeris model. By properly phasing each vehicle, it is possible for the formation to naturally evolve along this surface such that the relative positions of each spacecraft in the formation are unaltered and the relative distances are closely bounded. That is, if the formation originates as a string of pearls, the orientation of the string is relatively unaffected in time, the lead vehicle always remains in the lead and the order of each subsequent vehicle along the "string of pearls" remains unchanged. Since each spacecraft in this formation evolves along a naturally existing Lissajous trajectory, maintaining this type of formation can be achieved with a standard station keeping approach.

CONTINUOUS CONTROL IN THE EPHEMERIS MODEL

Previous studies by Howell and Marchand [18] demonstrate the efficiency and cost effectiveness of both input feedback linearization (IFL) and output feedback linearization (OFL) methods for continuous formation control in the CR3BP. The IFL controller is designed to force the error dynamics of each state variable to follow a critically damped response. The OFL controller, on the other hand, is applied only to force the radial separation between the spacecraft to track some specific value. Hence, no relative orientation requirements are imposed on the formation. The initial investigation [18] also demonstrates that a linear quadratic regulator (LQR), derived from optimal control theory, yields essentially an identical error response and control acceleration history as the input feedback linearization approach. However, the IFL controller is computationally much less intensive and, by comparison, conceptually simple. This particular characteristic makes the IFL controller more suitable for implementation in the ephemeris model than LQR.

In general, solving for the LQR gain matrix, over the duration of the mission, requires the solution of a two point boundary value problem. That is, the nonlinear equations of motion are subject to an initial boundary condition while the differential Riccatti equation is subject to a terminal boundary condition. In the CR3BP, the equations of motion are invariant under time transformation. Hence, it is possible to reduce the two-point boundary value problem to an initial value problem by appropriate choice of time transformation.

However, this property is not applicable to the ephemeris model and so, once again, solving the formation keeping problem via LQR techniques requires the solution of a two-point boundary value problem. The simplest way to accomplish this task requires that the nominal solution be stored and approximated on demand while solving the differential Riccatti equation. This process is extremely computationally intensive, particularly when multiple spacecraft are to be considered. Furthermore, there is a certain degree of error introduced by the interpolating polynomials. Reducing this error requires small integration step sizes which further decrease the integration speed.

Although LQR techniques are not easily implemented in the ephemeris model, both LQR and feedback linearization methods are still effective in achieving the formation keeping goals set forth in this investigation, as previously demonstrated. However, continued analysis of the OFL controller reveals some interesting features that were not apparent in the initial investigation. This analysis motivated the development of an optimal nonlinear controller, based on the OFL formulation. The solution to the resulting two point boundary value problem is obtained through a collocation method. To simplify the computational implementation of this method, the numerical results here are determined in the CR3BP. The various formulations of the OFL controller, however, are still applicable to the ephemeris model.

An example of continuous control, as applied here in the CR3BP model, is discussed from the perspective of a non-natural spherical formation. Because the formation of interest is now spherical, OFL is initially employed for control. Since an OFL controller tracks radial separation distances, this type of control may, in fact, be best suited for multi-spacecraft formations where each vehicle is constrained to evolve along the surface of a sphere centered on the chief spacecraft. However, a more detailed analysis of such controlled dynamics, beyond the scope of this paper, is necessary to assess if collisions between the vehicles in the formation arise.

Output Feedback Linearization

Previously [18], examination of the OFL controller focused on large formations characterized by relative separations of 5000 km. In terms of cost, and for this particular example, the resulting control effort that is required to achieve the goal is comparable to that of the input feedback linearization approach. However, the OFL controller has an added advantage in the sense that only radial distance needs to be controlled rather than the complete state vector, although naturally orientation control is lost. However, further analysis reveals that, as the nominal radial distance between the spacecraft decreases, the OFL controller can yield a significantly higher cost than that determined from IFL. Whether this increase is significant or not depends on the initial relative velocity of the deputy spacecraft.

In the three-body problem, recall that the equations of motion that govern the deputy dynamics can be represented as $\ddot{\bar{r}}(t) = \Delta\bar{f}\left(\bar{r}(t)\right) + \bar{u}(t)$, where $\Delta\bar{f}\left(\bar{r}(t)\right)$ denotes the net forces acting on the deputy, and $\bar{u}(t)$ is the control input. If this general equation is associated with the CR3BP, $\bar{r}$ represents the radial vector, measured relative to the chief spacecraft, in terms of rotating coordinates. The corresponding velocity and acceleration vectors, associated with the rotating frame, are denoted $\dot{\bar{r}}$ and $\ddot{\bar{r}}$, respectively. The OFL controller, originally formulated in [18], seeks to identify the control input $\bar{u}(t)$ such that $\ddot{r} = g\left(\bar{r}, \dot{\bar{r}}\right)$, where $g\left(\bar{r}, \dot{\bar{r}}\right)$ is representative of the desired critically damped radial error response. This leads to a single scalar constraint that can be represented in the form

$$h\left(\bar{r}(t), \dot{\bar{r}}(t)\right) = \bar{u}(t)^T \bar{r}(t). \tag{1.24}$$

where $h\left(\bar{r}, \dot{\bar{r}}\right)$ is some nonlinear function of $\bar{r}$ and $\dot{\bar{r}}$. The expression in Equation (1.24) represents one equation in three unknowns, the three control accelerations in the input vector $\bar{u}(t)$. Since no additional constraint equations are imposed, there are an infinite number of solutions that satisfy Equation (1.24). An immediately obvious solution to Equation (1.24) corresponds to a control history based solely on radial-axis inputs, termed here the "geometric" approach. That is, since $\bar{u}^T \bar{r} = ru\cos\theta$, where θ represents the angle between $\bar{u}$ and $\bar{r}$, it is obvious that $\bar{u} = \left\{h\left(\bar{r}, \dot{\bar{r}}\right)/r\right\}\hat{r}$ satisfies the constraint in (1.24). However, if the initial relative velocity, $\dot{\bar{r}}$, is large, this control law leads to absurdly high costs (16.3924 km/sec) and is therefore immediately disqualified as a viable option.

In the initial investigation into the OFL controller [18], the left side of Equation (1.24) is factored in terms of $\bar{r}(t)$ to allow for an explicit solution for $\bar{u}(t)$. Although this particular solution also satisfies the control goal, there are no guarantees or expectations of optimality. This formulation is based on the assumption that the measured output, $\bar{y}_1$, is defined as $\bar{y}_1 = \begin{bmatrix} r & \dot{r} \end{bmatrix}^T$. In the present study, two alternate output vectors are also considered, $\bar{y}_2 = \begin{bmatrix} r^2 & 2r\dot{r} \end{bmatrix}^T$ and $\bar{y}_3 = \begin{bmatrix} r^{-1} & -r^{-2}\dot{r} \end{bmatrix}^T$. Each of these output vectors leads to a different control law, as listed in Table 2. Furthermore, although all the resulting control laws achieve the formation goal, as specified, the associated formation keeping costs can be dramatically different, as previously noted. The controlled dynamics associated with each of these output vectors can also be very different, as deduced from Figure 19.

Clearly, the deputy spacecraft still evolves onto and along the surface of a sphere, but the manner in which this is accomplished varies according to the control law. For the OFL controllers, the dynamic response seems to always converge onto the same orbiting plane on the sphere. The motion of the deputy in response to the geometric controller (radial inputs only), on the other hand, eventually fills an entire region on the sphere. However, each controller leads to a different rotation rate about the chief spacecraft. That is, the

time to complete one orbital period on the surface of the formation sphere varies significantly with the controller, as illustrated in Figure 20. This is the reason why the associated formation keeping costs are so dramatically different across the four methods previously described. Since the controller only targets radial distance, the initial relative velocity of the deputy spacecraft, along with the choice of controller, essentially sets the rotation rate on the nominal formation sphere. For the controller formulations listed in Table 2, the orbital period can range between hours and days, as deduced from Figure 20. In contrast, a deputy spacecraft evolving along the natural formation surface illustrated in Figure 10 requires 180 days to complete one revolution.

Table 2 – Summary of Control Laws and Formation Keeping Costs (Over 180 days) for Various Output Vector Definitions

Output Vector	Control Law	Total Cost (m/sec) (180 Days)
$\bar{y}_1 = \begin{bmatrix} r \\ \dot{r} \end{bmatrix}$	$\bar{u}(t) = \left\{ \frac{g(\bar{r},\dot{\bar{r}})}{r} - \frac{\dot{\bar{r}}^T \dot{\bar{r}}}{r^2} \right\} \bar{r} + \left(\frac{\dot{r}}{r} \right) \dot{\bar{r}} - \bar{f}(\bar{r})$	2,310.5
$\bar{y}_2 = \begin{bmatrix} r^2 \\ 2r\dot{r} \end{bmatrix}$	$\bar{u}(t) = \left\{ \frac{1}{2} \frac{g(\bar{r},\dot{\bar{r}})}{r^2} - \frac{\dot{\bar{r}}^T \dot{\bar{r}}}{r^2} \right\} \bar{r} - \bar{f}(\bar{r})$	16,442.2
$\bar{y}_3 = \begin{bmatrix} r^{-1} \\ -r^{-2}\dot{r} \end{bmatrix}$	$\bar{u}(t) = \left\{ -rg(\bar{r},\dot{\bar{r}}) - \frac{\dot{\bar{r}}^T \dot{\bar{r}}}{r^2} \right\} \bar{r} + 3\left(\frac{\dot{r}}{r} \right) \dot{\bar{r}} - \bar{f}(\bar{r})$	49.8

To illustrate the impact that the relative velocity of the deputy has on the formation keeping cost, consider a nominal spherical formation characterized by a 5-km radial distance. Let $\bar{r}(0)$ and $\dot{\bar{r}}(0)$ denote the initial relative position and velocity vectors, respectively. For $\bar{r}(0) = 12\hat{x} - 5\hat{y} + 3\hat{z}$ km and $\dot{\bar{r}}(0) = \bar{0}$ m/sec the net formation keeping cost required to drive the deputy onto the surface of the nominal sphere is miniscule. However, as the relative velocity of the deputy increases, the OFL controller yields significantly higher costs. That is because the controller is trying to maintain a rotation rate specified by the initial velocity injection error, which is not consistent with the natural dynamics in the vicinity of the reference orbit. For the three output vectors defined in this study, the associated control inputs are summarized in Table 2. Also listed in Table 2 are the correction costs that correspond to an initial relative state defined by $\bar{r}(0) = 12\hat{x} - 5\hat{y} + 3\hat{z}$ km and $\dot{\bar{r}}(0) = \hat{x} - \hat{y} + \hat{z}$ m/sec. The associated nominal formation in this case is defined by a constant relative separation of 5 km.

The total formation keeping cost listed in Table 2 is determined by numerically integrating the net control acceleration over one orbital period of the reference halo orbit (180 days). Although the costs listed in Table 2 are unacceptable, they do indicate that, among the infinite number of control time histories that satisfy Equation (1.24), there likely is an optimal solution that is yet to be identified. The results presented in Table 2 motivate the development of an optimal nonlinear controller that accomplishes the goal of the OFL controller as previously defined.

Nonlinear Optimal Control Subject To Path and Control Input Constraints

Since the third case in Table 2 yields the lowest cost, this formulation is adopted as the basis for the derivation of a nonlinear quadratic regulator. As previously established with the OFL controller [18], the desired output dynamics correspond to a critically damped response of natural frequency ω_n,

$$\begin{aligned} &\frac{d^2}{dt^2}\left\{\frac{1}{r}\right\} = g\left(\bar{r},\dot{\bar{r}}\right) = -2\omega_n \frac{d}{dt}\left\{\frac{1}{r}\right\} - \omega_n{}^2\left\{\frac{1}{r}-\frac{1}{r_n}\right\}, \\ &g\left(\bar{r},\dot{\bar{r}}\right) = 2\omega_n\left\{\frac{\dot{\bar{r}}^T\bar{r}}{r^3}\right\} - \omega_n{}^2\left\{\frac{1}{r}-\frac{1}{r_n}\right\}. \end{aligned} \tag{1.25}$$

Evaluation of the second derivative on the left side of Equation (1.25) leads to

$$\frac{d^2}{dt^2}\left\{\frac{1}{r}\right\} = 3\frac{\left(\dot{\bar{r}}^T\bar{r}\right)^2}{r^5} - \frac{\bar{f}^T\bar{r}}{r^3} - \frac{\bar{u}^T\bar{r}}{r^3} - \frac{\dot{\bar{r}}^T\bar{r}}{r^3} = g\left(\bar{r},\dot{\bar{r}}\right). \tag{1.26}$$

Rearranging Equation (1.26) to isolate the control input $\bar{u}$ yields the a constraint of the form

$$h\left(\bar{r}(t),\dot{\bar{r}}(t)\right) - \bar{u}(t)^T\bar{r}(t) = 0, \tag{1.27}$$

as appeared previously where

$$h\left(\bar{r}(t),\dot{\bar{r}}(t)\right) = 3\left(\frac{\dot{\bar{r}}^T\bar{r}}{r}\right)^2 - \bar{f}\left(\bar{r}\right)^T\bar{r} - \dot{\bar{r}}^T\dot{\bar{r}} - r^3 g\left(\bar{r},\dot{\bar{r}}\right). \tag{1.28}$$

Note that this constraint is imposed on both the path and the control input.

Identifying an optimal nonlinear controller requires that the Euler-Lagrange theorem be applied to the nonlinear system with the addition of the constraint outlined by Equations (1.27)-(1.28). Since the path response is dictated by the expression in Equation (1.27), the cost function is simply given as

$$\min J = \int_{t_0}^{t_f} \frac{1}{2} \bar{u}(t)^T \bar{u}(t)\, dt\,. \tag{1.29}$$

In this case, the Hamiltonian is defined as

$$H = \frac{1}{2}\bar{u}^T\bar{u} + \bar{\lambda}_r\dot{\bar{r}} + \bar{\lambda}_v\left[\bar{f}(r) + \bar{u}(t)\right] + \mu\left(h\left(\bar{r},\dot{\bar{r}}\right) - \bar{r}^T\bar{u}\right). \tag{1.30}$$

The three-dimensional vectors $\bar{\lambda}_r$ and $\bar{\lambda}_v$ represent the co-states and the associated dynamics are governed by

$$\begin{bmatrix}\dot{\bar{\lambda}}_r \\ \dot{\bar{\lambda}}_v\end{bmatrix} = \begin{bmatrix}-\dfrac{\partial H}{\partial \bar{r}} \\ -\dfrac{\partial H}{\partial \dot{\bar{r}}}\end{bmatrix} = \begin{bmatrix}\mu\bar{u}(t) - \mu\dfrac{\partial h}{\partial \bar{r}} - \left(\dfrac{\partial \bar{f}}{\partial \bar{r}}\right)^T \bar{\lambda}_v \\ -\bar{\lambda}_r - \mu\dfrac{\partial h}{\partial \dot{\bar{r}}}\end{bmatrix}. \tag{1.31}$$

The optimal control law is then determined from

$$\frac{\partial H}{\partial \bar{u}} = \bar{0} = \bar{u}(t) + \bar{\lambda}_v - \mu\bar{r}\,, \tag{1.32}$$

thus,

$$\bar{u}(t) = \mu\bar{r} - \bar{\lambda}_v\,. \tag{1.33}$$

Note that Equations (1.27) and (1.33) represent four equations in four unknowns, $\bar{u}(t)$ and μ. From these expressions it is determined that

$$\mu = \frac{\left(h\left(\bar{r},\dot{\bar{r}}\right) + \bar{r}^T\bar{\lambda}_v\right)}{r^2}. \tag{1.34}$$

Finally, from the transversality condition, it is determined that the co-states must satisfy a zero terminal boundary condition. Since the equations of motion are subject to an initial condition, solving these equations and the co-state equations simultaneously requires the solution of a two-point boundary value problem (TPBVP). This implies that a solution must be iteratively determined based on some initial guess. Since the Euler-Lagrange theorem is based on the calculus of variations, it is assumed that the optimal solution is in the neighborhood of the initial guess and so, a good initial guess is critical in identifying the optimal solution to this problem. In this case, an initial guess is determined by numerically integrating the

state and co-state equations backwards from some pre-specified final time (12 hours). The co-states are defined as the elements of a zero vector at the beginning of the integration. The state vector, on the other hand, is assumed to have converged to the desired nominal, $\bar{r} = 5\hat{x}$ km and $\dot{\bar{r}} = \bar{0}$. The disadvantage of this approach is that the user has no control as to what particular initial state perturbs the response, but it at least provides a starting point. Using the collocation approach described by Shampine [33] and Kierzenka [33-34] all 12 equations are solved simultaneously, the converged solution is illustrated in Figure 21. The solid line represents the converged integrated trajectory while the circles denote the final converged location of the nodes used for the collocation method. Not surprisingly, the converged solution is consistent with one that is fixed in the rotating frame, since the specified final relative velocity is zero.

Although the collocation method worked well with the approach described above, it is extremely sensitive to changes in the initial conditions. This is not surprising considering the sensitivity to small perturbations characteristic in the *n*-body problem. So, identifying more efficient numerical methods to solve the nonlinear optimal control problem becomes a topic of interest during this investigation and is still under study. It is worth noting, however, that, in the *n*-body problem, these methods are computationally more suitable for the discrete control approach.

CONCLUSIONS

Previous studies demonstrate the efficiency of input and output feedback linearization in the continuous control of non-natural formations in the CR3BP. In the present analysis, these techniques prove to be equally effective in the more complete *n*-body ephemeris model, even in the presence of solar radiation pressure. Although the results here include only the gravitational effects of the Sun, the Earth, and the Moon, it is important to note that the influence of the remaining planets is easily incorporated into this model. The addition of these perturbations, however, has an insignificant impact on the formation keeping problem near the libration points, L_1 and L_2, of the Sun-Earth/Moon system.

Based on the available literature on continuous control, it is clear that linear and nonlinear techniques, such as LQR and feedback linearization, can mathematically enforce a non-natural configuration in the *n*-body problem. However, continuous thruster operation does not always represent a desirable option. The accelerations levels required to maintain a non-natural configuration are extremely small. Even with improved technology, the implementation error may be on the same order of magnitude as the thrust level, a potentially significant problem given the dynamical sensitivity to small perturbations. Precise formations, in fact, may not even be required, given a possible shift to improved navigation and relative position information. Hence, it is useful to explore the effectiveness of discrete control.

For non-natural formations, a basic targeter approach is implemented here to maintain the desired configuration within an acceptable level of accuracy. Not surprisingly, tightly spaced maneuvers are required to closely maintain a desired configuration. The frequency of the maneuver interval depends on the desired nominal separation between each spacecraft. Achieving the desired accuracy, and the physical requirements to do so, present yet another dilemma. As previously stated, if maintaining a tight non-natural formation is desired, frequent maneuvers are necessary. However, smaller maneuver intervals require smaller maneuvers. The magnitude of these maneuvers, individually, is still extremely small which, once again, raises an implementation issue.

The difficulties encountered with non-natural configurations may be overcome by developing a better understanding of the naturally existing formations. Although a nominal configuration completely consistent with the natural flow near the reference orbit is unlikely, understanding these naturally existing behaviors can lead to the development of techniques to construct formations to meet mission objectives that exploit the natural structure. To that end, a modified Floquet based controller is successfully applied here that reveals some interesting natural formations as well as deployment into these configurations.

ACKNOWLEDGEMENTS

This research was carried out at Purdue University with support from the Clare Boothe Luce Foundation and the National Aeronautics and Space Administration, Contract Number NAG5-11839.

REFERENCES

1. R.H. Vassar and R.B. Sherwood, "Formationkeeping for a Pair of Satellites in a Circular Orbit," *Journal of Guidance, Control, and Dynamics*, Vol. 8, Mar.-Apr. 1985, pp. 235-242.

2. D.C. Redding, N.J. Adams, and E.T. Kubiak, "Linear-Quadratic Stationkeeping for the STS Orbiter," *Journal of Guidance, Control, and Dynamics*, Vol. 12, Mar.-Apr. 1989, pp. 248-255.

3. Y. Ulybyshev, "Long-Term Formation Keeping of Satellite Constellation Using Linear Quadratic Controller," *Journal of Guidance, Control, and Dynamics*, Vol. 21, No. 1, Jan.-Feb. 1998, pp. 109-115.

4. V. Kapila, A. G. Sparks, J.M. Buffington, and Q. Yan, "Spacecraft Formation Flying: Dynamics and Control," *Journal of Guidance, Control, and Dynamics*, Vol. 23, No. 3, May-June 2000, pp. 561-563.

5. A. Sparks, *Satellite Formationkeeping Control in the Presence of Gravity Perturbations*. American Control Conference, Chicago, Illinois, June 28-30, 2000. Vol. 2 (A01-12740 01-63), Piscataway, New Jersey.

6. R.K. Yedevalli and A.G. Sparks, *Satellite Formation Flying Control Design Based on Hybrid Control System Stability Analysis*. American Control Conference, Chicago, Illinois, June 28-30, 2000, Proceedings. Vol. 3 (A01-12793 01-63), Piscataway, New Jersey.

7. D.J. Irvin Jr. and D.R. Jacques, "Linear vs. Nonlinear Control Techniques for the Reconfiguration of Satellite Formations," *AIAA Guidance, Navigation, and Control Conference and Exhibit*, Montreal, Canada, Aug. 6-9, 2001. AIAA Paper 2001-4089.

8. D.T. Stansbery and J.R. Cloutier, "Nonlinear Control of Satellite Formation Flight," *AIAA Guidance, Navigation, and Control Conference and Exhibit*, Denver, Colorado, Aug. 14-17, 2000. AIAA Paper 2000-4436.

9. S.R. Vadali, S.S. Vaddi, K. Naik, and K.T. Alfriend, "Control of Satellite Formations," *AIAA Guidance, Navigation, and Control Conference and Exhibit*, Montreal, Canada, Aug. 6-9, 2001. AIAA Paper 2001-4028.

10. S.R. Starin, R.K. Yedavalli, and A.G. Sparks, "Spacecraft Formation Flying Maneuvers Using Linear Quadratic Regulation with No Radial Axis Inputs," *AIAA Guidance, Navigation, and Control Conference and Exhibit*, Montreal, Canada, Aug. 6-9, 2001. AIAA Paper 2001-4029.

11. C. Sabol, R. Burns, and C. McLaughlin, "Satellite Formation Flying Design and Evolution," *Journal of Spacecraft and Rockets*, Vol. 38, No. 2, Apr. 2001, p. 270-278.

12. C.C. Chao, J.E. Pollard, and S.W. Janson, "Dynamics and Control of Cluster Orbits for Distributed Space Missions," Proceedings of the AAS/AIAA Space Flight Mechanics Meeting, Breckenridge, Colorado, Feb. 7-10, 1999. AAS Paper 99-126.

13. H. Schaub and K.T. Alfriend, "Impulsive Spacecraft Formation Flying Control to Establish Specific Mean Orbit Elements," *Journal of Guidance, Control, and Dynamics*, Vol. 24, No. 4, July-Aug. 2001, pp. 739-745.

14. Z. Tan, P. M. Bainum, and A. Strong, "The Implementation of Maintaining Constant Distance Between Satellites in Elliptic Orbits," *Advances in the Astronautical Sciences*, Vol. 105, 2000, pp. 667-683.

15. Z. Wang, F. Khorrami, and W. Grossman, *Robust Adaptive Control of Satellite Formationkeeping for a Pair of Satellites*, American Control Conference, Chicago, Illinois, June 28-30, 2000. Vol. 2 (A01-12740 01-63), Piscataway, New Jersey.

16. M.S. de Queiroz, V. Kapila, and Q. Yan, "Adaptive Nonlinear Control of Multiple S/C Formation Flying," *Journal of Guidance, Control, and Dynamics*, Vol. 23, No. 3, May-June 2000, p. 385-390.

17. Q. Yan, G. Yang, V. Kapila, and M.S. de Queiroz, "Nonlinear Dynamics and Output Feedback Control of Multiple Spacecraft in Elliptic Orbits," Proceedings of the American Control Conference, Chicago, Illinois, June 28-30, 2000, Vol. 2, Piscataway, New Jersey.

18. K.C. Howell and B.G. Marchand, "Control Strategies for Formation Flight in the Vicinity of the Libration Points," *AIAA/AAS Space Flight Mechanics Conference*, Ponce, Puerto Rico, Feb. 9-13, 2003. AAS Paper 03-113.

19. D.J. Scheeres and N.X. Vinh, "Dynamics and control of relative motion in an unstable orbit," *AIAA/AAS Astrodynamics Specialist Conference*, Denver, Colorado, Aug. 14-17, 2000. AIAA Paper 2000-4135.

20. P. Gurfil and N. J. Kasdin, "Dynamics and Control of Spacecraft Formation Flying in Three-Body Trajectories," *AIAA Guidance, Navigation, and Control Conference and Exhibit*, Montreal, Canada, Aug. 6-9, 2001. AIAA Paper 2001-4026.

21. P. Gurfil, M. Idan, and N. J. Kasdin, "Adaptive Neural Control of Deep-Space Formation Flying," *American Control Conference (ACC)*, Proceedings. Vol. 4, Anchorage, Alaska, May 8-10, 2002, p. 2842-2847.

22. R. J. Luquette and R. M. Sanner, "A Non-Linear Approach to Spacecraft Formation Control in the Vicinity of a Collinear Libration Point." *AAS/AIAA Astrodynamics Conference*; Proceedings, Quebec, July 30-Aug. 2, 2001, San Diego, California, p. 437-445.

23. N.H. Hamilton, "Formation Flying Satellite Control Around the L2 Sun-Earth Libration Point," M.S. Thesis, George Washington University, Washington, DC, December 2001.

24. D. Folta, J.R. Carpenter, and C. Wagner, "Formation Flying with Decentralized Control in Libration Point Orbits," International Symposium: Spaceflight Dynamics, Biarritz, France, June, 2000.

25. B.T. Barden and K.C. Howell, "Fundamental Motions Near Collinear Libration Points and Their Transitions," *The Journal of the Astronautical Sciences*, Vol. 46, No. 4, 1998, pp. 361-378.

26. B.T. Barden and K.C. Howell, "Formation Flying in the Vicinity of Libration Point Orbits," *Advances in Astronautical Sciences*, Vol. 99, Pt. 2, 1998, pp. 969-988.

27. B.T. Barden and K.C. Howell, "Dynamical Issues Associated with Relative Configurations of Multiple Spacecraft Near the Sun-Earth/Moon L1 Point," *AAS/AIAA Astrodynamics Specialists Conference*, Girdwood, Alaska, August 16-19, 1999, Paper No. AAS99-450.

28. K.C. Howell and B.T. Barden, "Trajectory Design and Stationkeeping for Multiple Spacecraft in Formation Near the Sun-Earth L1 Point," *IAF 50th International Astronautical Congress*, Amsterdam, Netherlands, Oct. 4-8, 1999. IAF/IAA Paper 99-A707.

29. G. Gómez, M. Lo, J. Masdemont, and K. Museth, "Simulation of Formation Flight Near Lagrange Points for the TPF Mission," AAS/AIAA Astrodynamics Conference, Quebec, Canada, July 30-Aug. 2, 2001. AAS 01-305.

30. K.C. Howell and T. Keeter, "Station-Keeping Strategies for Libration Point Orbits - Target Point and Floquet Mode Approaches," *Advances in the Astronautical Sciences,* Vol. 89, pt. 2, 1995, pp. 1377-1396.

31. G. Gómez, K.C. Howell, J. Masdemont, and C. Simó, "Station-keeping Strategies for Translunar Libration Point Orbits," *Advances in Astronautical Sciences*, Vol. 99, Pt. 2, 1998, pp. 949-967

32. C.R. McInnes, *Solar Sailing: Technology, Dynamics and Mission Applications*, United Kingdom: Praxis Publishing Ltd, 1999.

33. L.F. Shampine, J. Kierzenka, and M.W. Reichelt, *Solving Boundary Value Problems for Ordinary Differential Equations in Matlab Using bvp4c*, ftp://ftp.mathworks.com/pub/doc/papers/bvp/tutorial.pdf October, 2000.

34. J. Kierzenka, *Studies in the Numerical Solution of Ordinary Differential Equations*, Ph.D. Thesis, Southern Methodist University, Dallas, Texas, 1998.

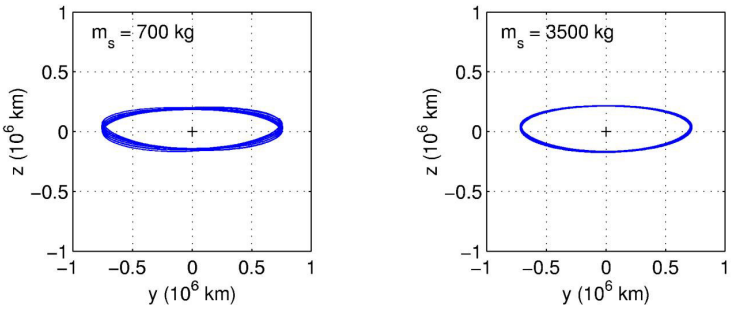

Figure 1 – Impact of S/C Mass and SRP Force on a Halo Orbit near L_2 in the Sun-Earth Ephemeris Model

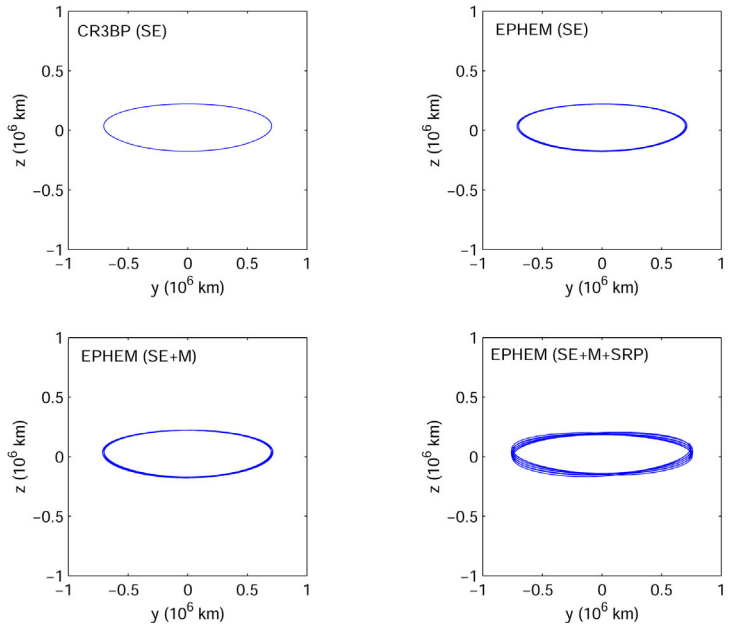

Figure 2 – Gravitational and Solar Radiation Pressure Effects on a Halo Orbit Near the Sun-Earth L_2 Point

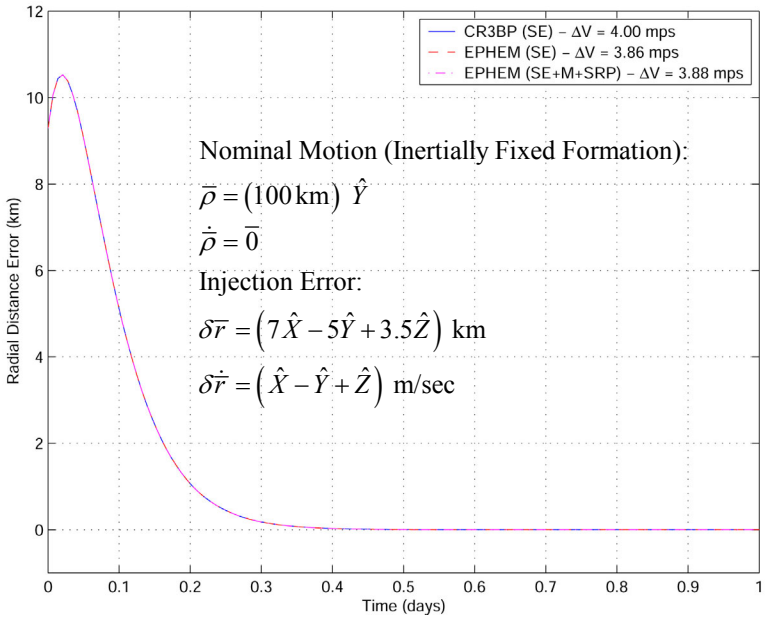

Figure 3 – IFL Response to Injection Error for Various Dynamical Models

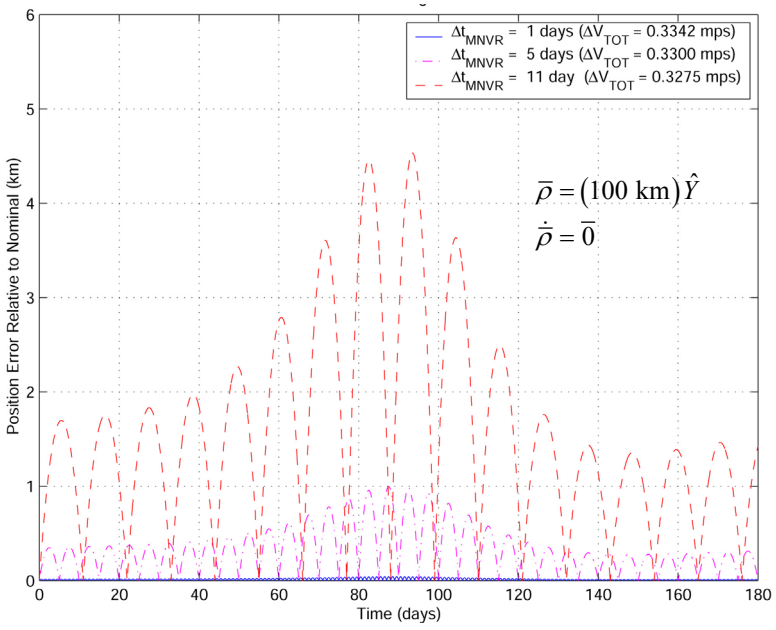

Figure 4 – Position Error Relative to the Nominal Path as a Function of the Length of the Maneuver Interval

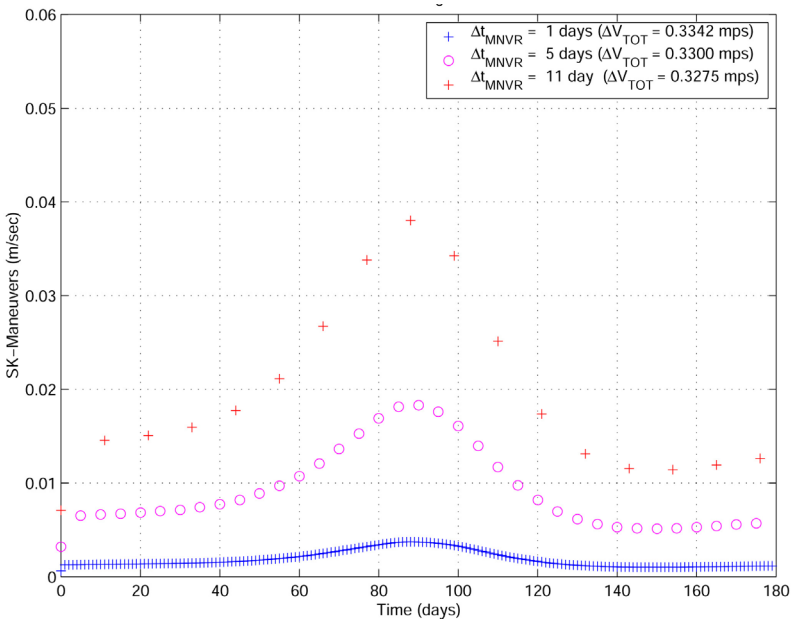

Figure 5 – SK Maneuver Strategy
(100-km 2-S/C Formation Aligned with Inertial *y*-axis)

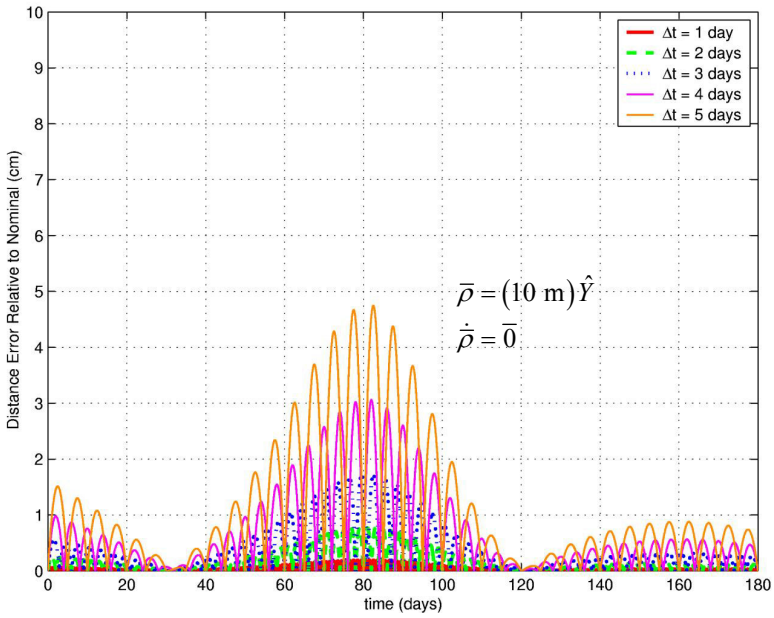

Figure 6 – Position Error Relative to the Nominal Path
as a Function of the Length of the Maneuver Interval

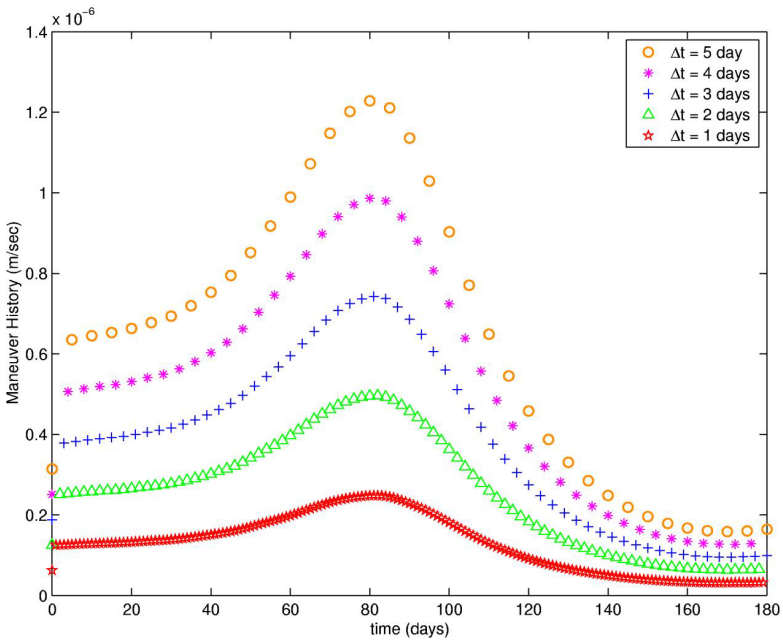

Figure 7 – SK Maneuver Strategy
(100-km 2-S/C Formation Aligned with Inertial *y*-axis)

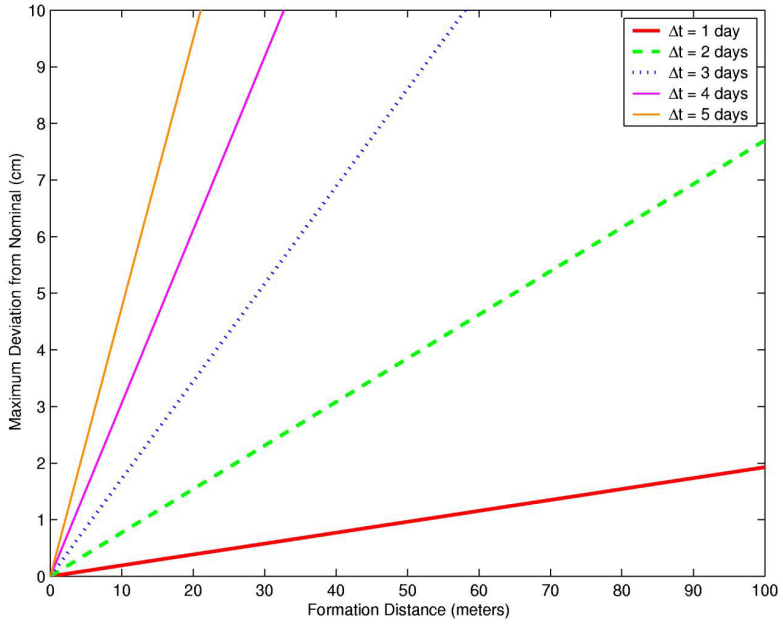

Figure 8 – Maximum Radial Deviation
as a Function of Nominal Formation Distance and Maneuver Time Interval

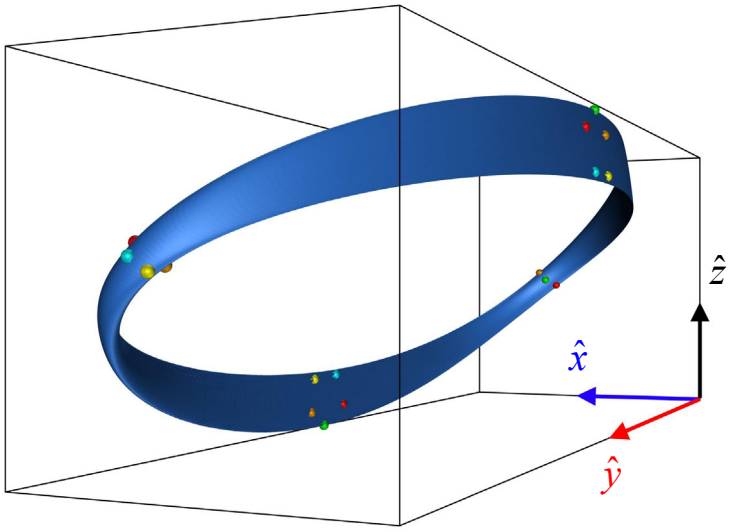

Figure 9 – Six Spacecraft Formation Evolving along Two-Dimensional Torus Near the Sun-Earth/Moon L_1. Point

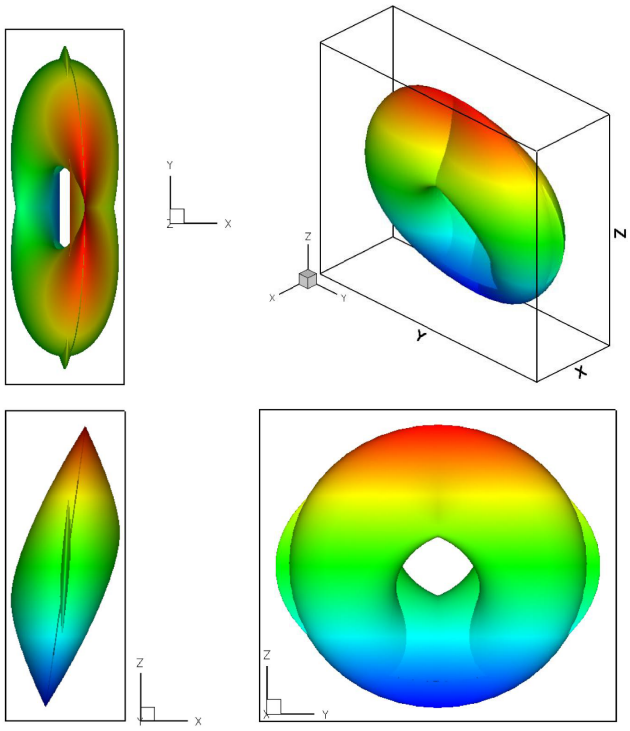

FIGURE 10 – Relative Deputy Motion along Center Manifold

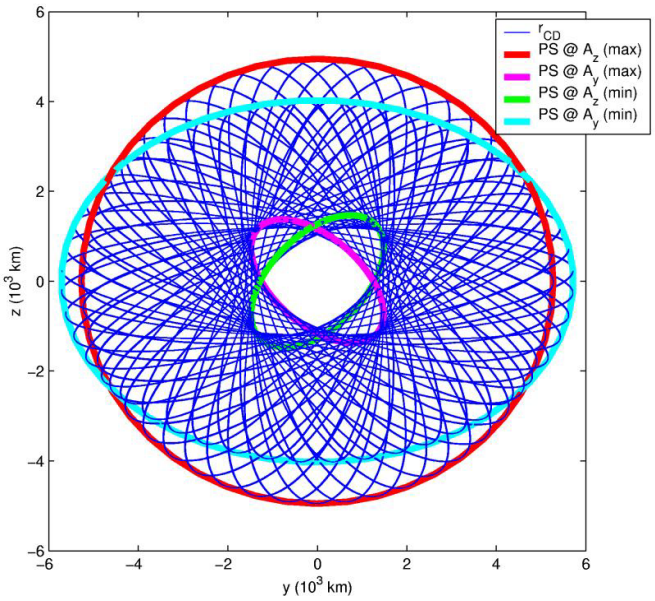

FIGURE 11 – Deputy S/C Location on Natural Formation Surface Sampled at Specific Locations along the Halo Orbit of the Chief S/C

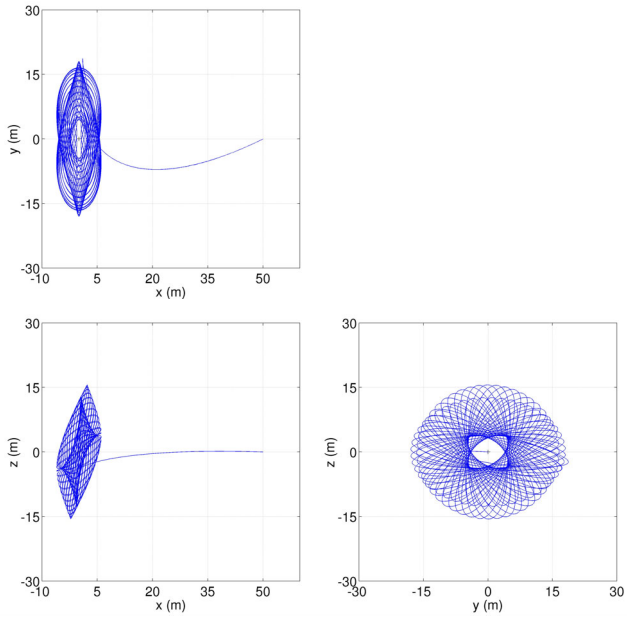

Figure 12 – Deployment into Toroidal Formation (Initial State Excites Only Modes 5 & 6)

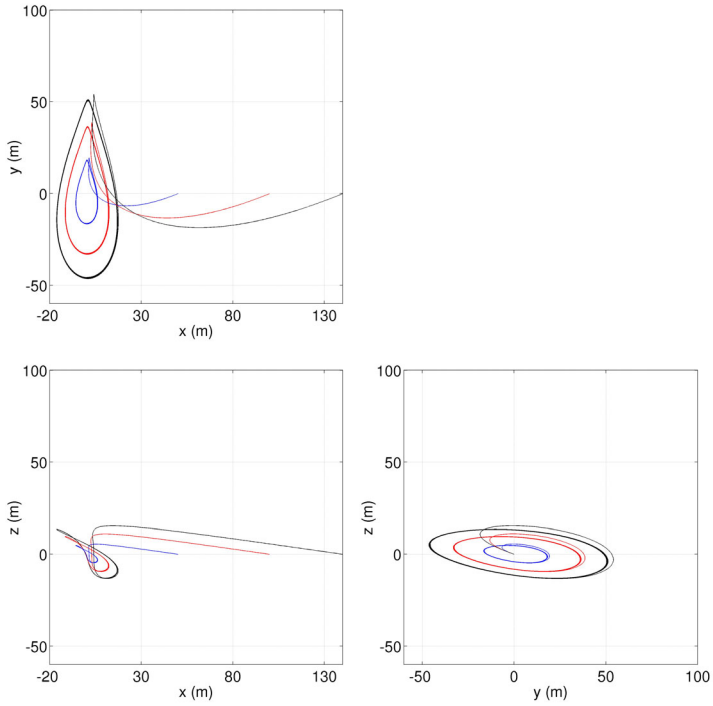

Figure 13 – Deployment into Nearly Periodic Formation

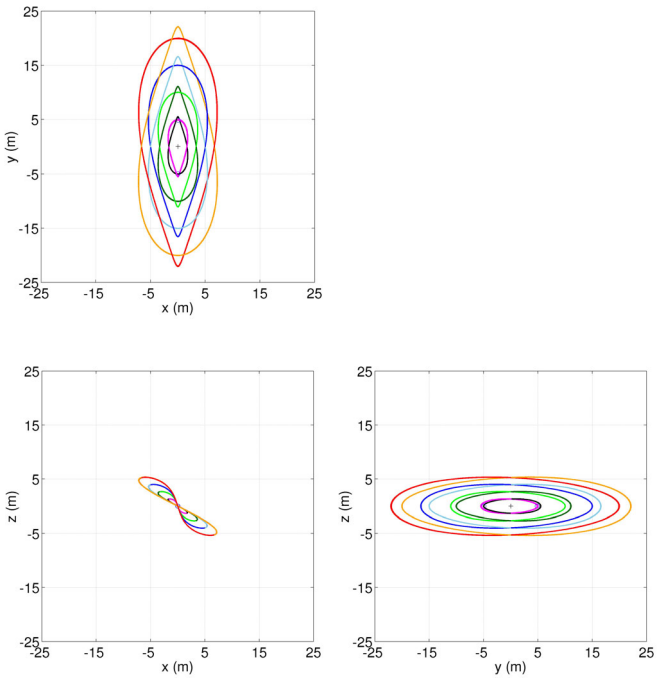

Figure 14 – Natural Eight Spacecraft Formation About a Single Chief S/C

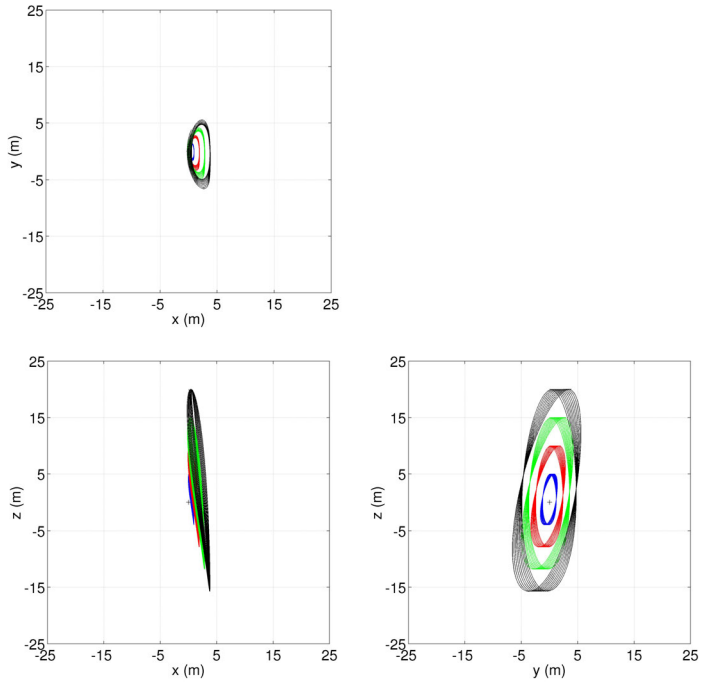

Figure 15 – Nearly Vertical Relative Orbits (4 S/C Formation)

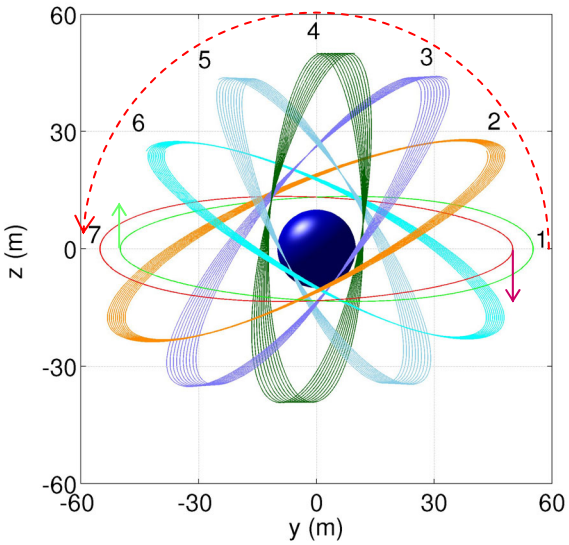

Figure 16 – Variation in Relative Orbit Expansion Rate Along the *yz*-plane

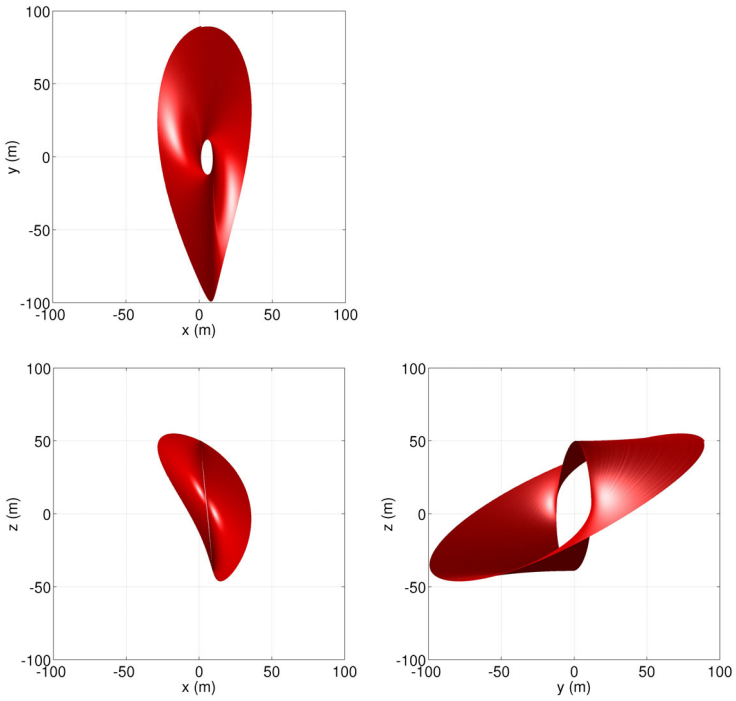

Figure 17 – Evolution of Nearly Vertical Orbit Over 100 Revolutions (49.2 Years)

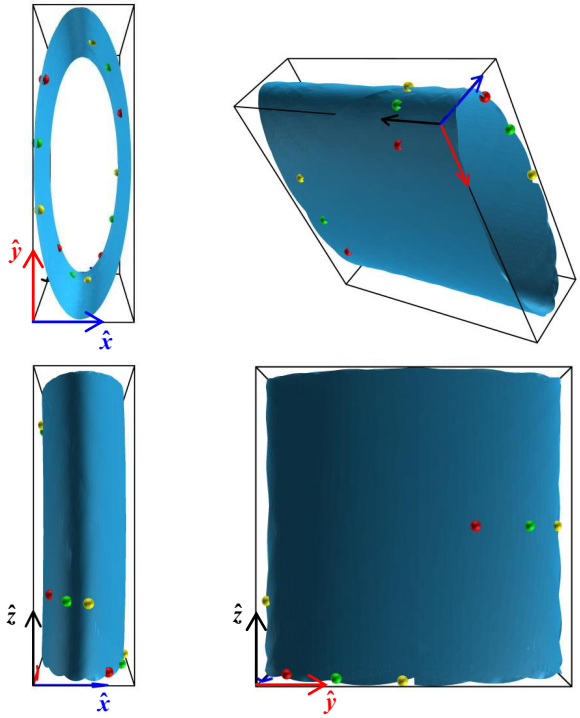

Figure 18 – Natural "String of Pearls" Formation in the Ephemeris Model

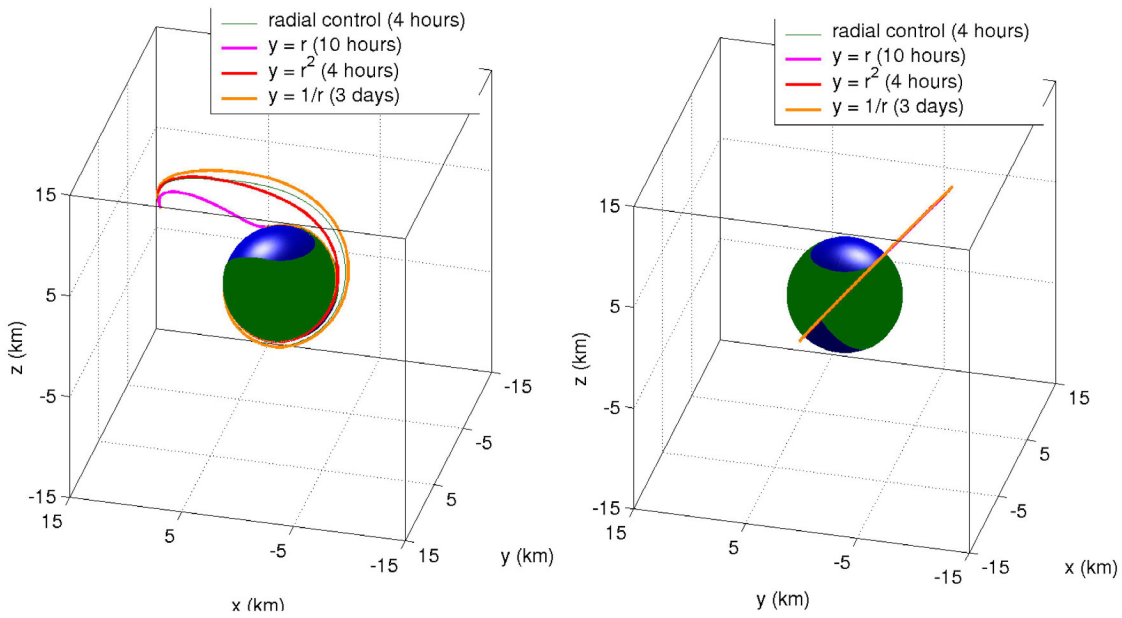

FIGURE 19 – Controlled Response of Deputy Path for PFL

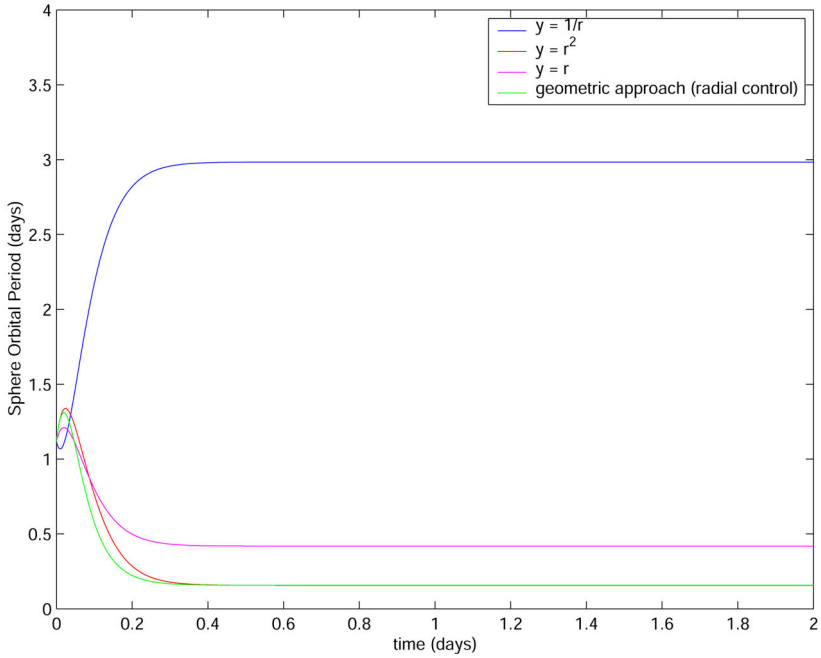

FIGURE 20 – Converged Rotation Rate for Spherical Formation Based on Four Different PFL Controller Formulations

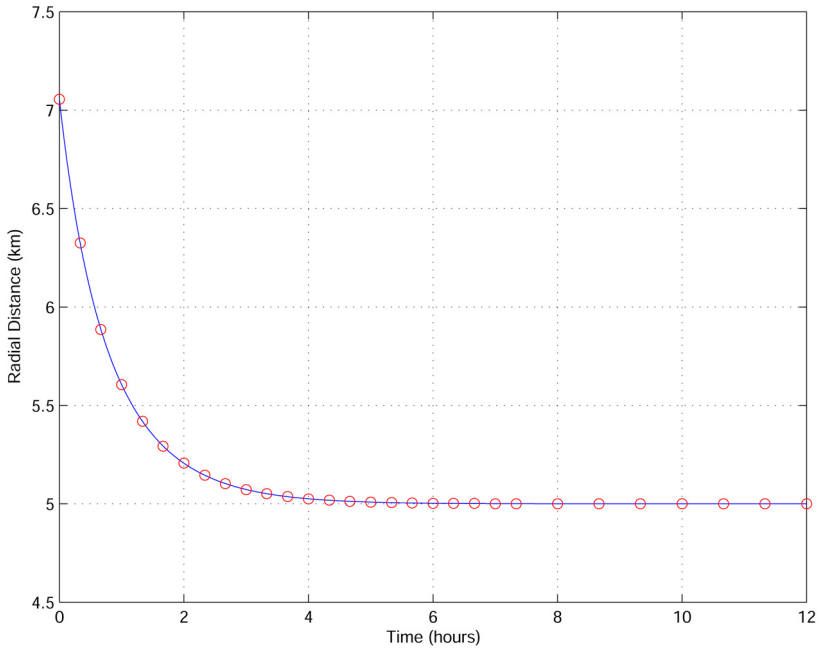

FIGURE 21 – Converged Optimal Response for OFL Controller